ORIGINAL RESEARCH PAPER

Removal of Crystal violet Dye from Aqueous Solution Using Surfactant Modified $NiFe_2O_4$ as Nanoadsorbent; Isotherms, Thermodynamics and kinetics Studies

Nina Alizadeh [1]*, Mohammad Mahjoub [2]

[1] *Department of Chemistry, University of Guilan, Rasht, Iran*

Received: 2017-03-23 Accepted: 2017-05-30 Published: 2017-06-25

ABSTRACT

The removal of crystal violet from aqueous solution by $NiFe_2O_4$ magnetic nanoparticles treated with sodium dodecyl sulfate was investigated. The modified magnetic nanoparticles were prepared by chemical reaction of a mixture of Ni^{+2} and Fe^{+3} ions mixture in aqueous solution in the presence of ammonia and then sodium dodecyl sulfate was utilized as an ionic surfactant to modify the obtained magnetic nanoparticles. The morphologies of synthesized magnetic nanoparticles were characterized by electron microscopy techniques. The X–ray diffraction results confirmed the formation of magnetic nanoparticles with face centered cubic structure and the crystallite size was found to be 19 nm. The Fourier transform infrared spectrums confirmed the coating of sodium dodecyl sulfate on synthesized magnetic nanoparticles. The effects of different parameters, such as pH, initial concentration of the dye and contact time were studied on the adsorption of crystal violet onto modified magnetic nanoparticles. The equilibrium data of dye adsorption were well fitted to the Freundlich adsorption isotherm. Adsorption kinetics was accommodated by a pseudo–second–order model and the results, obtained from Boyd plot indicated that the crystal violet adsorption onto modified magnetic nanoparticles was controlled by film diffusion. Thermodynamic parameters, such as changes in Gibbs free energy, enthalpy, and entropy were also determined. The calculated activation energy suggested physical adsorption of dye onto synthesized magnetic nanoparticles.

Keywords: *Crystal violet, $NiFe_2O_4$, Isotherm, Kinetic, Thermodynamic*

How to cite this article

Alizadeha N, Mahjoubb M. Removal of Crystal Violet Dye from Aqueous Solution Using Surfactant Modified $NiFe_2O_4$ as Nanoadsorbent; Isotherms, Thermodynamics and Kinetics Studies. J. Nanoanalysis., 2017; 4(1): 8-19.
DOI: 10.22034/jna.2017.01.002

INTRODUCTION

Recently, environmental pollution has been become a worldwide serious problem [1]. A large number of dyes discharge into the surface stream by many industries, such as textiles, plastics, paper rubber, tanning, cosmetics, pharmaceutical and foodstuff [2]. About 12% of synthetic textile dyes used each year is lost during manufacturing process and 20% of these dyes get into the environment through effluents [3]. Dye molecules are recalcitrant organic compounds, which are resistant to aerobic digestion and they have stability to light, heat and oxidizing agents due to their structures and molecular size and some of them are carcinogenic and mutagenic [4]. Crystal violet is a popular dye for its various purposes like biological stain, dermatological agent,

* Corresponding Author Email: n-alizadeh@guilan.ac.ir, TelFax: +98 (013)33333262

and veterinary industrial products [5]. Crystal violet is a mutagen and mitotic poison which may cause cancer and can cause severe eye irritation through ingestion or skin contact [6]. So, the removal of crystal violet from aqueous solutions is essential to human health and water resource protection. There are many methods for dye removing like cloud point extraction [7], photocatalytic degradation [8], biodegradation [9] and electrochemical degradation and electrocoagulation [10]. But all of these methods do not have good acceptability because of many restrictions. Adsorption has been discovered to be superior to other techniques for dye removing because of advantages like low coast, ease of operation and efficiency [11]. Since the adsorption process is directly dependent on the quality of the adsorbent, in the recent year's researchers has been paid attention to improve the effective quality of adsorbents in different forms, such as activated carbon [12], zeolites [13], Composite [14], lignocelluloses [15], natural minerals [16] and functioned polymers [17]. However, most of these adsorbents have been shown some problems like high cost, difficulties of separation from wastewater and generation of secondary wastes [11]. Scientists combined the magnetic separation technique and nanotechnology to perform the adsorption of dyes from aqueous solutions [18].

In the proposed method, the sodium dodecyl sulfate (SDS) molecules were used as surfactant coordinating their functional group on the MNPs. Hence, the hydrophobic carbon tail of SDS molecules was pointed outwards from the surface of the synthesized MNPs. The hydrophobic chains on the surface of MNPs produced stable suspensions in solvents and prevent from self–aggregation. Modified MNPs have been shown additional advantages like the ease of synthesis and manipulation via subsequent coating and functionalization, no secondary pollutants, cost effectiveness and environmental friendliness [11, 19]. Therefore, the purpose of this work was to introduce the adsorption potential of $NiFe_2O_4$–SDS MNPs for crystal violet as a cationic dye from aqueous solutions. The equilibrium, kinetic and thermodynamic data of the adsorption process were studied to understand the adsorption mechanism of crystal violet onto the surface of the modified MNPs in the optimum conditions.

EXPERIMENTAL

All chemicals and reagents used in this study were of analytical grade and used without further purification. Deionized water was used throughout the reactions. A stock solution of 0.1 M of crystal violet was prepared by dissolving 2.039 g of dye in 50 ml deionized water and it was used freshly.

The UV–Vis spectra were recorded using 6715 Jenway spectrophotometer. Transmission electron microscopy (TEM) and scanning electron microscopy (SEM) studies were performed using a Philips CM30 and VEGA\TESCAN–XMU, respectively. Fourier transform infrared (FT–IR) spectra were recorded at room temperature using Bruker FT–IR spectrometer. X–ray diffraction (XRD) patterns were obtained using a MPD3000/GNR diffractometer.

Synthesis of $NiFe_2O_4$–SDS MNPs

The starting reagents, 14.4 g of $Ni(NO_3)2.6H_2O$ and 26.6 g of $Fe(NO_3)_3.9H_2O$, were dissolved in 20 ml of deionized water and then 10 ml of NH3 (%30 V/V) was added drop wise using to the prepared solution under stirring with a vertical glass stirrer. During the whole process, the temperature of the solution was maintained at 45°C. The obtained $NiFe_2O_4$ MNPs were separated from the reaction medium via magnetic field and the obtained MNPs were washed with sufficient deionized water for three times, then they were dried at 40°C for 2 days and after this time MNPs were heated at 350°C in the furnace for 1 hour. Continuing heating of MNPs, eventuate to elimination of NOX gases and formation of $NiFe_2O_4$. The obtained $NiFe_2O_4$ was grind and added to the 2 ml of SDS %5 W/V solution, with vigorous stirring for 5 minutes and After 10 minutes as rest time, the $NiFe_2O_4$–SDS MNPs were separated by magnetic field and dried.

Removal of Crystal Violet Using $NiFe_2O_4$–SDS MNPs

Batch equilibrium studies were carried out by adding a fixed amount of $NiFe_2O_4$–SDS MNPs (0.1 g) into 25 ml of crystal violet solution (with different initial concentration) in 50 ml of the Erlenmeyer flask at room temperature. The mixture was centrifuged at 130 rpm for 50 minutes as adsorption time. The $NiFe_2O_4$–SDS MNPs were quickly separated from the sample solution using a high power magnet (1.2 T). The equilibrium concentration of crystal violet was determined by measuring the absorbance using UV–Vis spectrophotometer at 590 nm. The residual dye concentration in the solution was determined via spectrophotometric method using a calibration curve. The resulting data were used to evaluate the adsorption of crystal violet onto $NiFe_2O_4$–SDS MNPs at equilibrium and named with qe (mg of dye/g of adsorbent)

$$q_e=(C_0-C_e)V/W \quad (1)$$

Where C0 and Ce (mg L–1) are the concentration of crystal violet at initial and equilibrium, respectively, V (L) is the volume of the sample solution and W (g) is the mass of dry adsorbent used. The percentage of crystal violet removal was calculated using the following equation

$$\%R=((C_0-C_t))/C_0\times100 \quad (2)$$

Where, Ct is the equilibrium concentration after t minute from the initiation of the reaction.

RESULT AND DISCUSSION

Characterization of $NiFe_2O_4$–SDS MNPs

XRD Studies

To identify the structure, composition and size of $NiFe_2O_4$ MNPs, XRD patterns were used (figure 1). The XRD peaks appearing at 2θ values 30.12°, 35.52°, 37.12°, 43.24°, 53.56°, 57.32° and 62.84° could be attributed to the 220, 311, 222, 400, 422, 511 and 440 crystallographic planes. It can be indexed as face centered cubic structure of $NiFe_2O_4$, according to the standard JCPDS (card No. 10–0325).

The average size of the synthesized $NiFe_2O_4$ MNPs was estimated ffrom the Debyee–Scherrer formula [20]:

$$D=0.94\lambda/\beta\cos\theta \quad (3)$$

Where λ is wavelength of XRD (0.1514 nm), β is full width at half maximum, θ is the diffraction angle and D is the particle diameter size. The average size of synthesized $NiFe_2O_4$ MNPs was computed to be 19 nm. Spurious diffractions appeared in XRD pattern was related to crystallographic impurities [21].

SEM and TEM Studies

The morphology and the size of the $NiFe_2O_4$ and $NiFe_2O_4$–SDS MNPs were determined by SEM and TEM, respectively (figure 2). The TEM and SEM images indicated that the position of synthesized MNPs was highly influenced by SDS and at the absence of SDS molecules, the self–aggregation of MNPs was occurring. This indicates that, the molecules of SDS could play an important role like capping reagent and prevent the MNPs to be self–aggregation. From the TEM images, it was observed that the quasi spherical synthesized MNPs were in the average size ranging about 10–20 nm, which is in close agreement with the size obtained from XRD analysis.

FT–IR Study

The FT–IR spectra of synthesized $NiFe_2O_4$ and $NiFe_2O_4$–SDS is shown in figure 3. The peak at 664 and 598 cm^{-1} are related to the Fe–O group [18]. These two bands are usually assigned to the vibration of ions in crystal lattice indicating the presence of uniformly distributed ferrite particles. The band at 664 cm^{-1} corresponds to intrinsic stretching vibration of the metal at the tetrahedral site [22]. The peaks at 1632 cm^{-1} represent H–O–H bending vibration of water. The broad peak at 3453 cm^{-1} is assigned to OH group could be attributed to OH stretching vibration of H_2O absorbed by the MNPs and the surface OH [23].

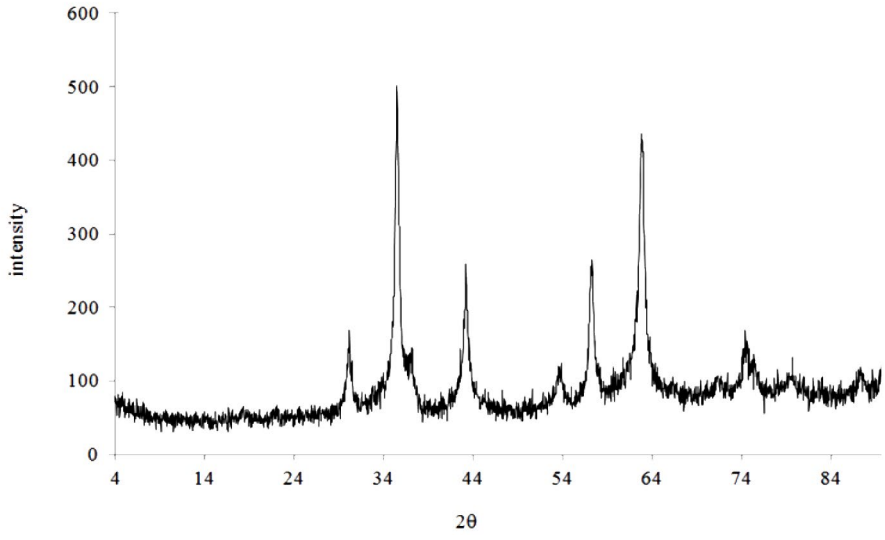

Fig. 1. XRD pattern of synthesized $NiFe_2O_4$ MNPs (V: 40 KV, I: 30 mA, Lamp: Cu).

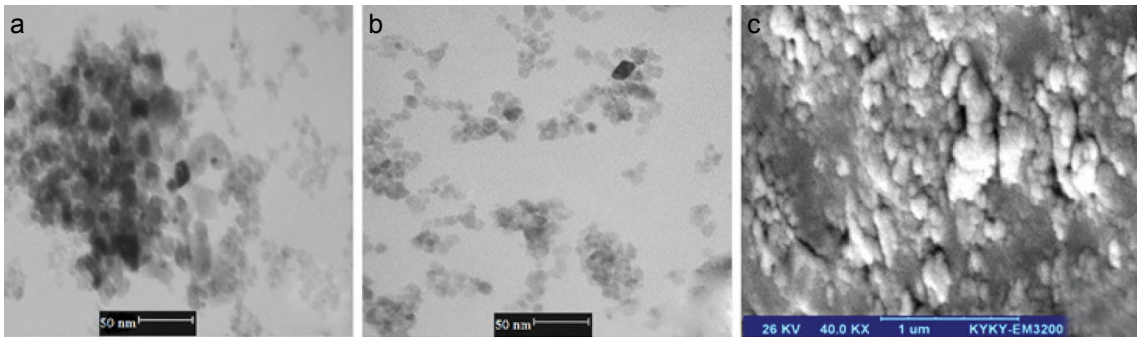

Fig. 2. TEM images of synthesized $NiFe_2O_4$ MNPs (a) and coated MNPs with SDS (b) (scale 50 nm). SEM images of synthesized $NiFe_2O_4$ MNPs (scale: 500 nm) (c).

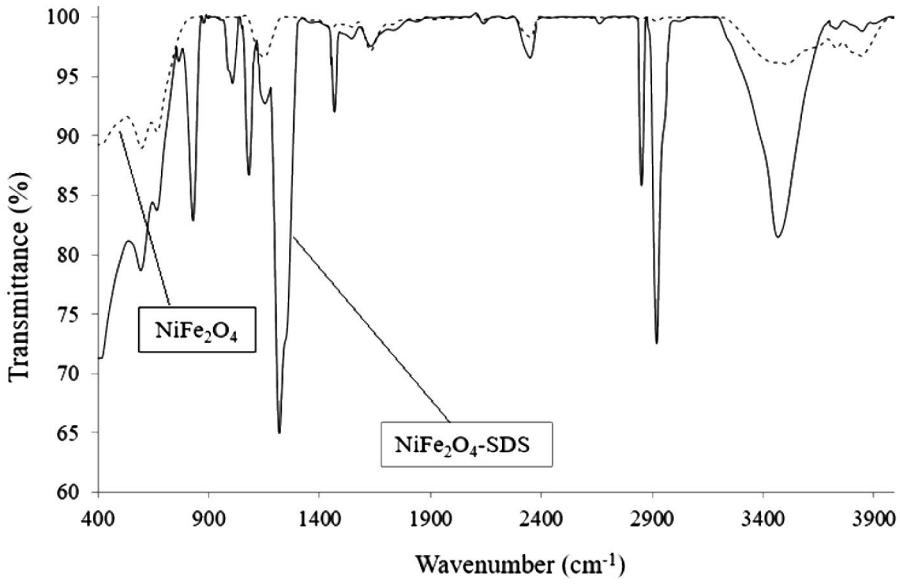

Fig. 3. FT–IR spectra of synthesized $NiFe_2O_4$ MNPs (dash line) and $NiFe_2O_4$–SDS MNPs (continues line).

The FT–IR spectra of modified MNPs showed that the new peaks are related to the presence of SDS molecules. The peak near 3465 cm^{-1} represents the bending vibration of adsorbed molecular water. A peak at 2925 cm^{-1} indicated the asymmetric stretching vibration of CH_3, and peak assigned to asymmetric and symmetric stretching of CH_2 were found at 2850 cm^{-1}, respectively. The asymmetric and symmetric deformation vibrations of CH_3 were found at 1470 and 1225 cm^{-1}, respectively. The peaks for asymmetric and symmetric stretching of the S=O of SDS were found at 1010 and 1085 cm^{-1}, respectively. The peak at 850 cm^{-1} was assigned to the asymmetrical stretching vibration of C–O–S. Thus, it has been clear that the presence of functional groups of SDS molecules on the surface of adsorbent due to coating phenomenon of MNPs by SDS molecules with Van der Waals forces or weak electrostatic interaction [23, 24].

Removal of Crystal Violet Dye with $NiFe_2O_4$–SDS MNPs

To achieve maximum adsorption efficiency of crystal violet on modified MNPs, various parameters were studied and optimized. At first, the effect of pH on the crystal violet adsorption on $NiFe_2O_4$–SDS MNPs was studied in solution with dye concentration of 30 mg L–1 at pH range 2 to

8. The pH value of dye solution plays an important role in the whole adsorption process. It was found that the percentage of dye removal increased by increasing in the pH of solution from 2 to 5.5 and fall down at higher pH values. In acidic pH values, the molecules of dye are in their cationic form, so they can interact with the negatively charged surface of $NiFe_2O_4$–SDS MNPs. From other side, at lower pH values the H^+ ions can contend with the cationic from of dye molecules. At the basic pH values, the surfaces of synthesized MNPs are negatively charged and the molecules of dye are negative, too. Therefore, the dye molecules cannot directly interact with MNPs. This behavior clearly suggests that the adsorption is dominated by the interaction between SDS and adsorbent surface.

Figure 4 illustrates the data obtained from studying the adsorption process of crystal violet by $NiFe_2O_4$–SDS MNPs. The efficiency of dye removal was increased as the agitation time increased and lowers initial dye concentration. As can be seen from figure 4, the amount of the absorbed crystal violet at low initial concentration achieve to equilibrium after 25 minutes from the initiation of reaction, while at higher initial concentration, the equilibrium time increased to 35 minutes, thereafter it reached to a constant value where no more dye could be removed from the solution. This phenomenon was due to the fact that at initial stage, a large number of surface site were available for adsorption. After a lapse of time, the remaining sites are difficult to be reached because of the repulsion force between the adsorbed ions of crystal violet and free ions of dye in bulk phases. In fact, the crystal violet molecules have to first encounter the boundary effect and then diffuse from boundary layer film onto adsorbent surface. Finally, it has to diffuse into the porous structure of the adsorbent surface [25]. Therefore, the experimental data were measured at 50 minutes of the initiation of the reaction to be sure that full equilibrium attained. The results show that, an increase in initial concentration of crystal violet dye leads to increase in the adsorption of dye on $NiFe_2O_4$–SDS MNPs. The average percent of adsorption capacity (qe) at equilibrium was obtained 0.408, 2.004, 3.758 and 5.195 mg g^{-1} for initial concentration of 1, 5, 10 and 15 mg L^{-1}, respectively. This indicates that the initial dye concentration provided a powerful driving force to overcome the mass transfer resistance between the aqueous solution of dye and solid phase of adsorbent.

In figure 5, the modification process of MNPs with SDS and the suggested mechanism for adsorption of crystal violet onto modified MNPs was illustrated, clearly.

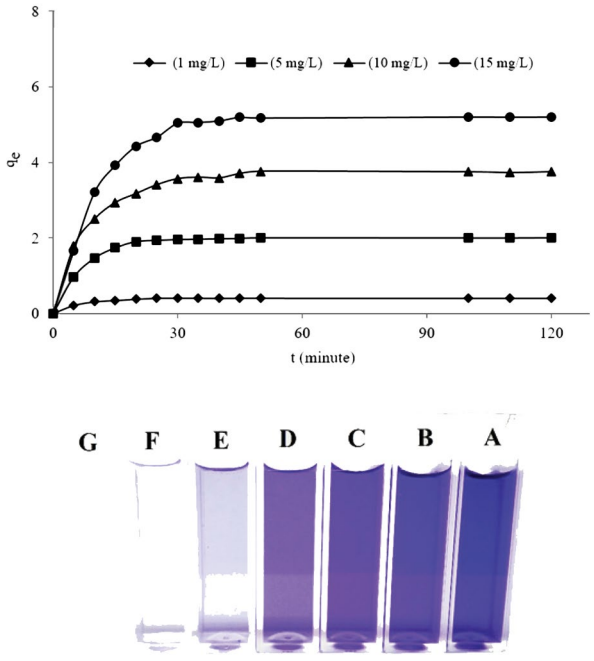

Fig. 4. FT–IR spectra of synthesized $NiFe_2O_4$ MNPs (dash line) and $NiFe_2O_4$–SDS MNPs (continues line)

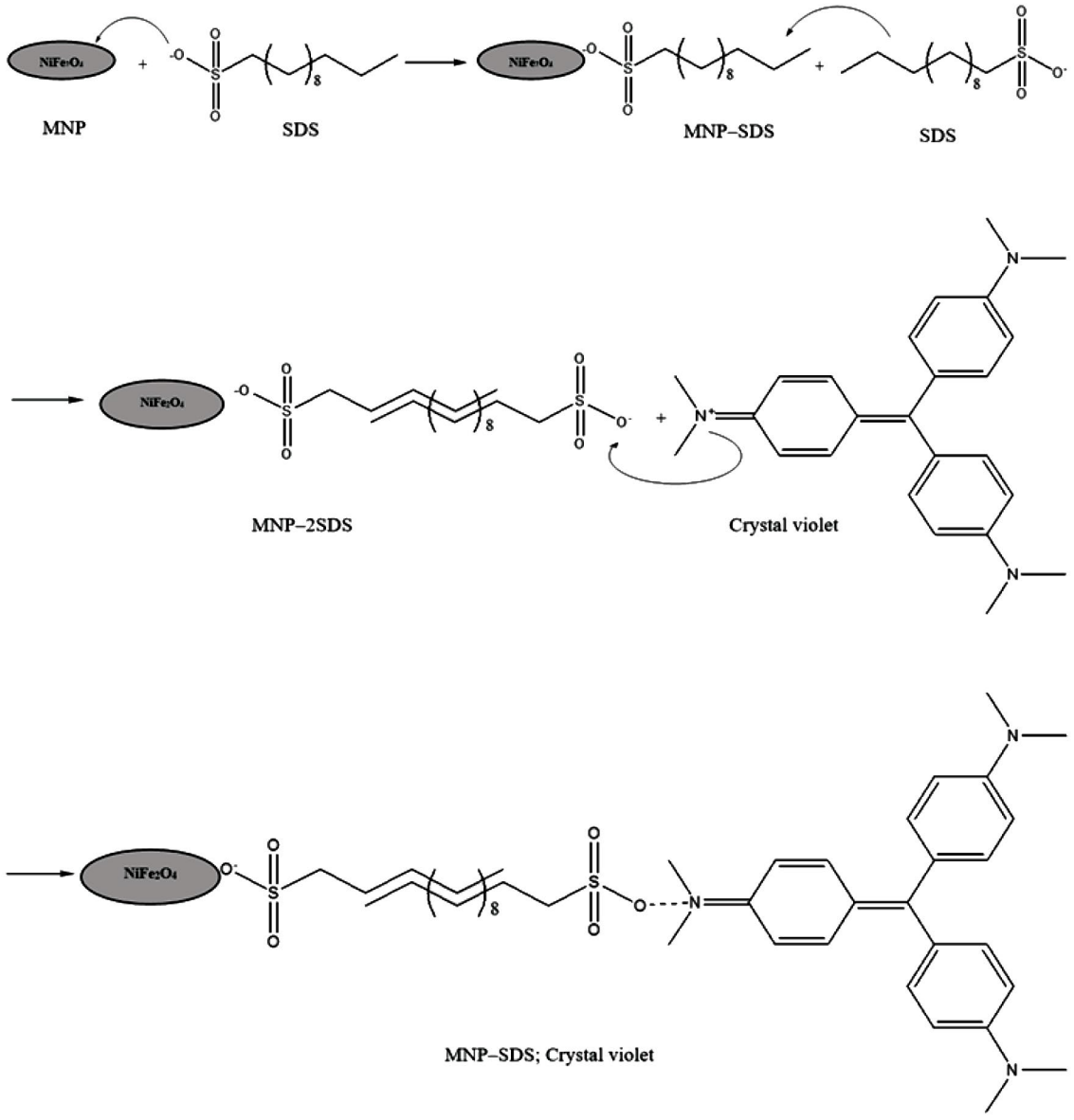

Fig. 5. The scheme is illustrating the modification process used to coat $NiFe_2O_4$ MNPs with SDS and suggested mechanism of adsorption of crystal violet onto $NiFe_2O_4$–SDS MNPs.

Adsorption Isotherms

The dye adsorption process at the solid–liquid interface could be described by the following steps: (i) diffusion of dye molecules from bulk solution to the adsorbent surface through the boundary layer (film diffusion), (ii) diffusion of dye ions from the surface into the pores of the solid particles (pore diffusion or intraparticle diffusion) and (iii) interaction of dye with the active sites on the surface of the adsorbent [26]. Several theoretical models have been suggested to describe the kinetic model of diffusion. Here, five kinetic models, Langmuir, Freundlich, Temkin, Flory–Huggins and Dubinin–Radushkevich (figure 6 B–F) were tested for their ability to describe the experimental results. The fitness of these models was evaluated by the regression coefficients (R^2) value.

The Longmuir adsorption isotherm assumes that

adsorption takes place at specific homogeneous site within the adsorbent and it has found successful application for many processes of monolayer adsorption [18]. The Freundlich isotherm model is based on adsorption on the heterogeneous surface of varied affinities [25]. The Temkin isotherm model is based on the assumption that the heat of adsorption would decrease linearly with increasing of adsorbent coverage [18]. Flory–Huggins isotherm model which occasionally deriving the degree of surface coverage characteristics of adsorbate onto adsorbent, can express the feasibility and spontaneous nature of an adsorption process [27]. Dubinin–Radushkevich isotherm is an empirical model which is initially conceived for the adsorption of subcritical vapors onto micro pore solids. It is generally applied to express the adsorption mechanism [28].

In Langmuir adsorption isotherm assumes that the monolayer adsorption (the adsorbed layer is one molecule in thickness), with adsorption can only occur at a finite (fixed) number of definite localized sites, that are identical and equivalent, with no lateral interaction between the adsorbed molecules, even on adjacent sites [25]. The mathematical expression of Langmuir isotherm models is illustrated in Table 1. The essential characteristic of Longmuir equation can be expressed in terms of dimensionless factor, commonly known as a separation factor (R_L).

$$R_L=1/((1+K_L C_0)) \quad (4)$$

Where, C_o is the highest initial concentration of solution. In this context, lower R_L value reflects that adsorption is more favorable. In a deeper explanation, R_L value indicates the adsorption nature to be either unfavorable (R_L >1), linear (R_L=1), favorable (0< R_L <1) or irreversible (R_L=0) [25, 27]. The computed R_L values versus the initial concentration of crystal violet at different temperature are shown in figure 6 A. The obtained results show that the R_L values are between 0 and 1, which confirms that the adsorption phenomenon was favorable.

Freundlich isotherm is the earliest known relationship describing the non–ideal and reversible adsorption, not restricted to the formation of monolayer. This empirical model can be applied to multilayer adsorption, with nonuniform distribution of adsorption heat and affinities over the heterogeneous surface. The magnitude of the exponent, 1/n, gives an indication of the favorability of adsorption. The values of n>1 represent favorable adsorption conditions [29]. During this investigation, the values of n are greater than 1 and display the same trend at all studied temperatures. The results indicate adsorption nature of crystal violet on $NiFe_2O_4$–SDS MNPs are favorable.

Temkin isotherm contains a factor that explicitly taking into the account of adsorbent–adsorbate interactions. By ignoring the extremely low and large value of concentrations, the model assumes that the heat of adsorption (function of temperature) of all molecules in the layer would decrease linearly rather than logarithmic with coverage [25]. In the present study, the Temkin plot was plotted between qe versus lnCe. The values of bT and AT were obtained and tabulated from the slope and intercept of Temkin plot, respectively.

Flory–Huggins isotherm model which occasionally deriving the degree of surface coverage characteristics of adsorbate onto adsorbent, can express the feasibility and spontaneous nature of an adsorption process. In some literature [30] the value of the Flory–Huggins isotherm constant (KFH) was used for calculation of spontaneity free Gibbs energy.

$$\Delta G^0=-RT \ln(K_{FH}) \quad (5)$$

But in this research, the value of KL was used for computing the values of free Gibbs energy [23]. The values of nFH and KFH were calculated in three studied temperatures and they were tabulated in Table 1.

Dubinin–Radushkevich isotherm is generally applied to express the adsorption mechanism [28] with a Gaussian energy distribution onto a heterogeneous surface. The approach was usually applied to distinguish the physical and chemical adsorption of metal ions. In this isotherm, the parameter of Polany potential (£) can be correlated as:

$$\varepsilon=RT \ln[1+1/C_e] \quad (6)$$

One of the unique features of the Dubinin–Radushkevich isotherm model lies on the fact that it is temperature dependent.

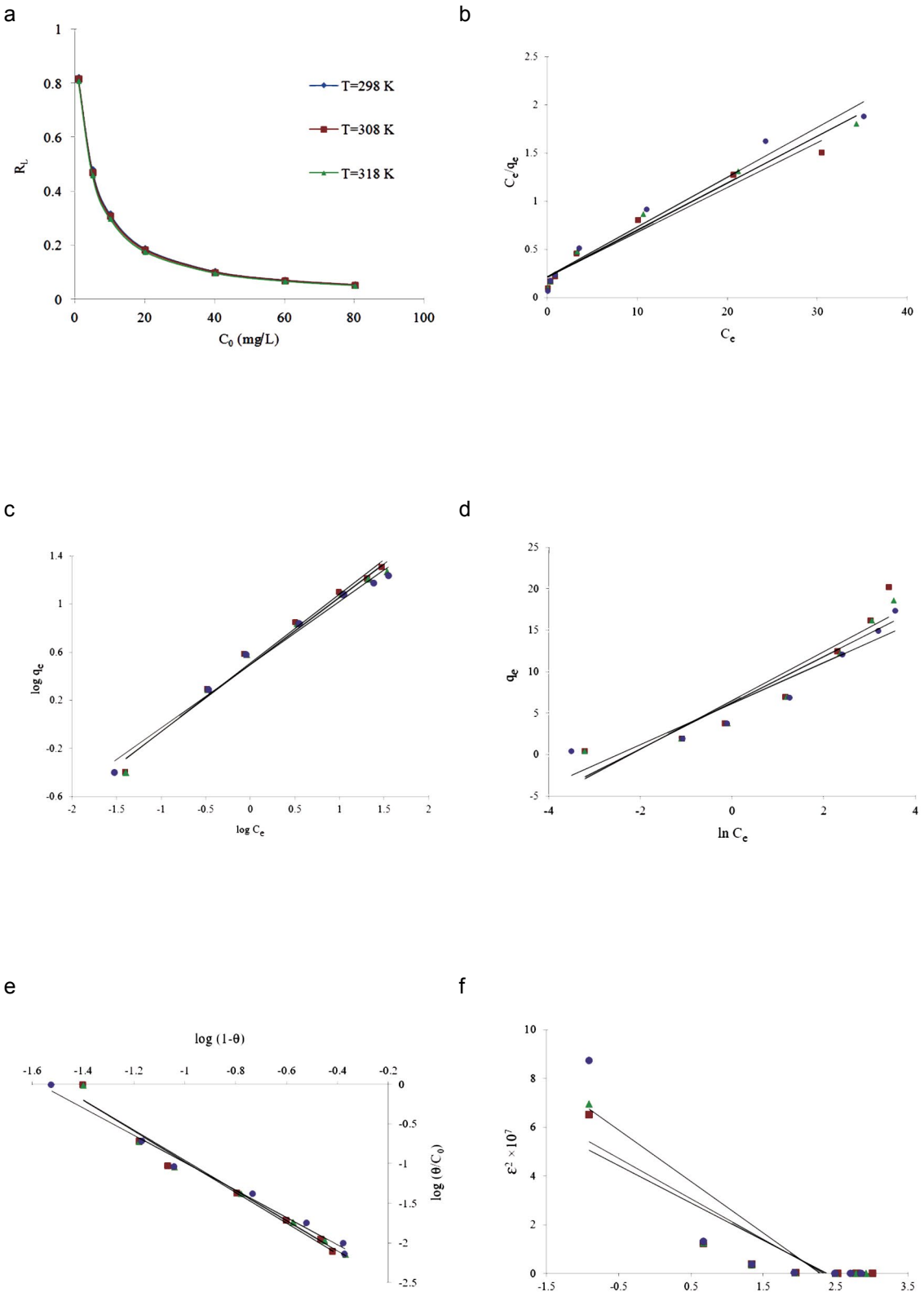

Fig. 6. Effect of crystal violet concentrations on separation factor (a). Adsorption isotherm plots of crystal violet onto synthesized $NiFe_2O_4$–SDS MNPs: Longmuir (b), Freundlich (c), Temkin (d), Flory–Huggins (e) and Dubinin–Radushkevich (f).

Table 1. Equations and parameters of the adsorption isotherm models for crystal violet adsorption onto $NiFe_2O_4$–SDS MNPs (initial concentration of dye: 1, 5, 10, 20, 40, 60 and 80 mg L^{-1} and R_L calculated for C_0=10 mg L^{-1})

Isotherm model	Non–linear form	Linear form	Parameters		T (298K)	T (308K)	T (318K)
Longmuir	$q_e=((Q_0 K_L C_e))/((1+K_L C_e))$	$C_e/q_e=1/(Q_0 K_L)+1/Q_0 C_e$	**q_e** (adsorbed amount of dye); **C_e** (concentration of dye in equilibrium state); **Q_0** (monolayer adsorption capacity); **K_L** (Longmuir adsorption constant)	Q_0	21.46	20.49	19.34
				K_L	0.217	0.224	0.236
				R_L	0.316	0.308	0.298
				R^2	0.9641	0.9770	0.9680
Freundlich	$q_e=K_F C_e^{1/n}$	$logq_{-e}=logK_F+1/n\ logCe$	**K_F** (Freundlich adsorption coefficient) and **1/n** are fitting constant	n	1.748	1.791	1.902
				K_F	3.266	3.146	3.157
				R^2	0.9842	0.9819	0.9832
Temkin	$q_e=RT/b_T\ lnA_T C_e$	$q_e=RT/b_T\ lnA_T+(RT/b_T)\ lnC_e$	**R** (gas constant); **T** (temperature); **b_T** (constant parameter related to the heat of adsorption); **A_T** (Temkin isotherm constant)	b_T	824.65	921.75	1072.1
				A_T	8.89	9.67	12.22
				R^2	0.8797	0.8971	0.8961
Flory–Huggins	$\theta/C_0=K_{FH}(1-\theta)^{nFH}$	$log(\theta/C_0)=log(K_{FH})+n_{FH}\ log(1-\theta)$	**n_{FH}** (ions number occupying sites); **K_{FH}** (Flory Huggins isotherm constant); (degree of surface coverage)	n_{FH}	–1.94	–1.90	–1.72
				K_{FH}	1.19×10^{-3}	1.36×10^{-3}	1.95×10^{-3}
				R^2	0.9748	0.9783	0.9897
Dubinin–Radushkevich	$q_e=(q_s)\ e((^{-kad\ \varepsilon 2}))$	$ln(q_e)=ln(q_s)-k_{ad}\ \varepsilon^2$	**$_s$** (the maximum amount adsorbed); **$_{ad}$** (activity coefficient related to mean adsorption energy); (Polany potential)	q_s	38.34	49.04	124.91
				k_{ad}	1.534	1.657	2.107
				R^2	0.7901	0.7886	0.7780

Adsorption Kinetics

The adsorption kinetic study is important to predict the mechanisms (chemical reaction or mass transport process) which control the rate of dye removal and retention time of adsorbed species. In order to analyze the adsorption kinetics of crystal violet onto $NiFe_2O_4$–SDS MNPs, four kinetic models; pseudo–first–order, pseudo–second–order, intraparticle diffusion (Weber–Morris) and Boyd models (Figure 7 A–D) were applied.

Linear plot of $ln(q_e–q_t)$ against t in Lagergren equation (pseudo–first–order) and the plot of t/qt versus t in Ho and Mckay model (pseudo–second–order), allow us to obtain the experimental values of calculated q_e, k_1 and k_2 from slops and intercepts, respectively. Whichever were found to be linear with better correlation coefficient (closer to 1), this indicated that the equation was appropriate to crystal violet adsorption onto $NiFe_2O_4$–SDS MNPs. From Table 2, the obtained R2 value of pseudo–second–order model was close to unity. Besides, the best model fit was evaluated based on values of the difference between values of the calculated and experimental adsorption capacities values by means of root mean square (RMS) error analysis [31] as follows:

$$RMS=\sqrt{(\sum\_(i=1)N[((q\_calc-q\_exp))/q\_exp]2)/N} \quad (7)$$

Where qcalc and qexp correspond to calculating and experimental adsorption capacity, respectively,

and N is the number of experimental points. From equation 7, the values of RMS for pseudo–first–order and pseudo–second–order models were calculated to be 0.171 and 0.109, respectively. These facts indicate that the adsorption of dye on nanoparticles fitted well to pseudo–second–order model.

In order to get information about the diffusion mechanism, the kinetic results were analyzed by the intraparticle diffusion model. The qt versus t0.5 will be linear if the intraparticle diffusion occurs. The rate limiting process is only due to the intraparticle diffusion if the plot passes through the origin. The multi–linearity of the plots in Weber–Morris model indicates that two or more steps influence on the adsorption process [25]. Different lines of intraparticle diffusion plot did not cross the origin. It suggests that some boundary layer control contributes to the adsorption process, confirming that intraparticle diffusion is not the only rate limiting step [31].

To suggest the slow step involved in the adsorption process, the kinetics data were also subjected to Boyd kinetics model analysis. As can be seen from figure 7 B, the relation between B_t and t (minute) was linear, approximately. But the straight line did not pass through the origin, which indicates that the crystal violet adsorption onto $NiFe_2O_4$–SDS MNPs is mainly controlled by a film diffusion mechanism. The values of B (slope of the straight line obtained from the Boyd plot) can be used to calculate the effective diffusion coefficient with the following equation [27]

$$B=(\pi^2 D_i)/r^2 \quad (8)$$

Where r (cm) is the radius of the adsorbent particle (assuming spherical shape) and Di (cm^2 s^{-1}) is the effective diffusion coefficient.

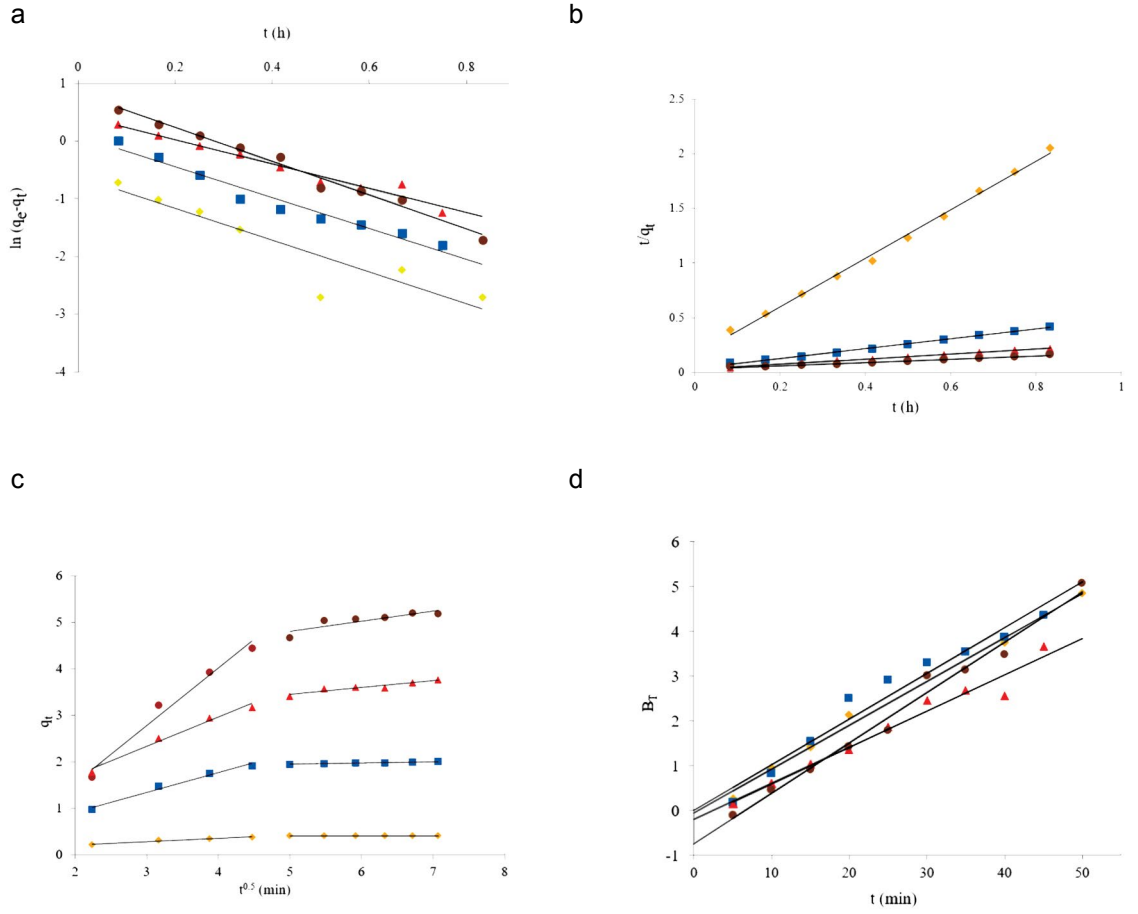

Figure 7. The pseudo–first–order (a), pseudo–second–order (b), Intraparticle diffusion model (c) and Boyd (d) plots for the adsorption of crystal violet onto $NiFe_2O_4$–SDS MNPs (initial concentration of dye: 1, 5, 10 and 15 mg L^{-1}; T: 298K)

Table 2. Equations, parameters and finding results of the pseudo–first–order, pseudo–second–order, Intra particle diffusion and Boyd kinetic models for the adsorption of crystal violet onto $NiFe_2O_4$–SDS MNPs at 298K

Kinetic model	Equation	Fundamental characteristic	Kinetic parameters		Concentration of crystal violet (mg L^{-1})			
				1	5	10	15	
pseudo–first–order (Lagergren)	$\ln(q_e-q_t)=\ln-q_e-k_1 t$	**q_e** and **q_t**: the amounts of adsorbate adsorbed at equilibrium (mg g^{-1}); **t**: time (h); **k_1**: adsorption rate constant (1/t)	$q_{experimental}$		0.408	2.004	3.758	5.195
			$q_{calculated}$		0.238	1.22	2.829	6.669
			k_1		6.308	6.142	4.874	6.757
			R^2		0.8429	0.9599	0.9670	0.9836
pseudo–second–order (Ho–Mckay)	$t/q_t=1/(k_2 q_e^2)+1/q_e t$	**k_2**: rate constant of second–order adsorption (g mg^{-1} t^{-1}); **h, ()**: initial adsorption rate	$q_{calculated}$		0.448	2.223	4.269	6.506
			k_2		32.265	5.747	2.069	0.856
			h		6.501	28.400	37.718	36.232
			R^2		0.9962	0.9962	0.9991	0.9870
Intraparticle diffusion (Weber–Morris)	$q_t=k_{pi} t^{0.5}+C_i$	**k_{pi}**: the rate parameter of stage I (mg g^{-1} $t^{0.5}$); **C_i**: represent the boundary layer effect	I	k_{pi}	0.0727	0.4206	0.629	1.2318
				C	0.0636	0.0763	0.4368	0.9224
				R^2	0.961	0.9795	0.9818	0.9734
			II	k_{pi}	–0.0007	0.0298	0.1494	0.2163
				C	0.411	1.7915	2.693	3.723
				R^2	0.06	0.9841	0.8976	0.7541
Boyd	B_t=-0.4977-$\ln(1-F)$	F=(q_t/q_e): fraction of solute adsorbed at any time	B		0.0982	0.0102	0.082	0.1126
			D_i		9.96×10^{-9}	1.03×10^{-9}	8.23×10^{-9}	1.14×10^{-8}
			R^2		0.9933	0.9599	0.9670	0.9836

Adsorption Thermodynamics

In order to determine the thermodynamic feasibility and the thermal effects of the adsorption, Gibbs free energy (ΔG°), entropy (ΔS°) and enthalpy (ΔH°) were calculated. The values of ΔG° can be computed from the following equation [23]

$$\Delta G°=-RT\ \ln K\_L \quad (9)$$

Where T (K) is the temperature of solution, KL is the Longmuir isotherm constant and R (8.314 J mol^{-1} K^{-1}) is the universal gas constant. From Arrhenius equation [25], the activation energy of adsorption was evaluated using the equation 10

$$\ln k\_2=\ln A-E\_a/RT \quad (10)$$

Where k_2 is the rate constant obtained from the pseudo–second–order kinetic model.

The values of ΔH° and ΔS° can be obtained from the following equation [25]:

$$\ln K_L=\Delta S°/R-\Delta H°/RT \quad (11)$$

From equation 11, the values of ΔH° and ΔS° can be calculated from the plot of lnKL versus 1/T (Vant–Hoff Plot). The calculated values of ΔG°, ΔS°, ΔH° and Ea for adsorption of crystal violet dye onto synthesized $NiFe_2O_4$–SDS MNPs are summarized in Table 3.

Table 3. Thermodynamic parameters for the adsorption of crystal violet onto $NiFe_2O_4$–SDS MNPs

–ΔG° (kJ mol^{-1})			ΔH° (kJ mol^{-1})	ΔS° (J mol^{-1} K^{-1})	E_a (kJ mol^{-1})
298 K	308K	318K	–3.160	–0.5712	7.848
2.999	2.965	2.989			

The negative values of ΔG° indicate the spontaneous nature of the adsorption process of the selected range

of temperature. The negative values of enthalpies show that the adsorption process was exothermic in nature. The negative values of entropies were related to the low affinity of the dye molecules toward the MNPs and decreasing randomness at the solid/solution interface with some structural and steric changes in the crystal violet and synthesized MNPs during the adsorption process [25]. The positive value of activation energy shows the conceivability of the adsorption process. From the other side, the calculated eye is lower than 40 KJ Mol^{-1}. It shows that the rate determining step in the adsorption process should be physically controlled.

CONCLUSION

The synthesis and characterization of $NiFe_2O_4$ MNPs treated with SDS are reported that was developed as an efficient adsorbent for the removal of crystal violet from aqueous solutions. From the SEM, TEM, FT–IR and XRD techniques, the morphology, size (19 nm), synthesis processes and coating phenomenon of MNPs were investigated, respectively. It was found that, the adsorption of crystal violet onto $NiFe_2O_4$–SDS reached to equilibrium at 25 min at lower concentration (1, 5 mg L^{-1}) and 35 min at higher concentrations (10, 15 mg L^{-1}) and at suitable pH values. Crystal violet adsorption on modified MNPs showed an increase by increasing the contact time, temperature and initial concentration of dye. Adsorption kinetics was followed the pseudo–second–order model and the Freundlich isotherm displayed best fitting curve between five isotherm model used. The plots of intraparticle diffusion model were revealed that the adsorption process occurred in two steps and the activation energy from the Arrhenius equation suggested that physical adsorption was the major mechanism which was controlled the adsorption of crystal violet on modified MNPs.

CONFLICT OF INTEREST

The authors declare that there is no conflict of interests regarding the publication of this manuscript.

ACKNOWLEDGMENT

Financial support from the research affairs of university of Guilan is acknowledged. The authors are grateful for the Qazvin water board company, Qazvin, Iran, for the immaterial supplementary protection.

REFERENCES

1. J. Paul, K.P. Rawat, K.S.S Sharma and S Sabharwal, Appl. Radiat. Isotopes, 69, 982 (2011).
2. M. Stolte and M Vieth, Acta. Endosc., 31, 125 (2001).
3. C. Smaranda, M. Gravilescu and D. Bulgrin, Int. J. Environ. Res., 5, 177 (2011).
4. C. Supdita, Bioresource Technol., 101, 1800 (2010).
5. A. Adak, M. Bandyopadhyay and A. Pal, Dyes Pig., 69, 251 (2006).
6. D.B. Jirekar, G. Pramila and M. Farooqui, Int. J. Chem. Tech. Res., 15, 427(2014).
7. A. Appusamy, I. John, K. Ponnusamy and A. Ramalingam, Eng. Sci. Technol., 17, (2014).
8. S. Ameen, M.S. Akhtar, M. Nazim and H.S. Shin, Mater. Lett., 96, 228 (2013).
9. G.K. Parshetti, S.G. Parshetti, A.A. Telke, D.C. Kalyani, R.A. Doong and S.P. Govindwar, J. Environ. Sci., 23, 1384 (2011).
10. R.E.P. Goyes, F.L.G. Duque, G. Penuela, I. Gonzalez, J.L. Nava, R.A.T. Palma, J. Chemosphere., 81, 26 (2010).
11. F. Keyhanian, S. Shariati, M. Faraji and M. Hesabi, Arab J. Chem., 9, 348 (2011).
12. M.S. Shafeeyan, W.M.A. Wan–Daud, A. Houshm and A. Shamiri, J. Anal. Appl. Pyrol., 89, 143 (2010).
13. M.R. Panuccio, A. Sorgona, M. Rizzo, G. Cacco, J. Environ. Manage., 90, 364 (2009).
14. Y.R. Jiang, H.P. Lin, W.H. Chung, Y.M. Dai, W.Y. Lin and C.C. Chen, J. Hazard. Mater., 283, 787 (2015).
15. E.W. Shin, K.G. Karthikeyan and M.A. Tshabalala, Bioresource. Technol., 98, 588 (2007).
16. K. Sevgi, Desalination, 244, 24 (2009).
17. G.C. Panda, S.K. Das and A.K. Guha, Colloid Surf. B., 62, 173 (2008).
18. A. Ebrahimian–Pirbazari, E. Saberikhah and S.S. Habibzadeh–Kozani, Water Resources and Industry, 7, 23 (2014).
19. M. Gholami, M.T. Vardini and G.R. Mahdavinia, Carbohyd. Polym., 136, 772 (2016).
20. J. Rita and S.S. Florence, J. Chalcogenide. Lett., 7, 269 (2010).
21. R. Varshney, S. Bhadauria and M.S. Gaur, Adv. Mat. Lett., 1, 237 (2010).
22. S.R. Ramesh, A. Ramanand, S. Ponnusamy and C. Muthamizhchelvan, Appl. Surf. Sci., 258, 6648 (2012).
23. P. Rai, R.K. Gautam, S. Banergee, V. Rawat and M.C. Chattopadhyaya, Environ. Chem. Eng. J., 3, 2281 (2015).
24. R. Moghadam, M.Z.B. Hussein and Y.H. Taufiq, Int. J. Mol. Sci., 13, 13275 (2012).
25. M.A. Ahmad and R. Alrozi, Chem. Eng. J., 171, 510 (2011).
26. D. Suteu and T Malutan, Bioresources, 8, 427 (2013).
27. K.Y. Foo and B.H. Hameed, Chem. Eng. J., 156, 2 (2010).
28. A. Gunay, E. Arslankaya, I. Tosun, J. Hazard. Mater., 146, 362 (2007).
29. B.H. Hameed, J.M. Salman and A.L. ferr, J. Hazard. Mater., 163, 121 (2009).
30. K. Vijayaraghavan, T.V.N. Padmesh, K. Palanivelu and M. Velan, J. Hazard. Mater., B 133, 304 (2006).
31. B.C.S. Ferreira, F.S. Teodoro, A.B. Mageste, L.F. Gil, R.P. de–Freitas and L.V.A. Gurgel, Industrial corps and products, 65, 521 (2015).